中国激光

声学分辨的双侧激发光声显微成像技术

曾思略[1,3]，刘良检[1]，陈涛[1]，方驰华[3]，刘成波[1**]，郑海荣[2*]

[1]中国科学院深圳先进技术研究院生物医学光学与分子影像研究室，广东 深圳 518055；

[2]中国科学院深圳先进技术研究院劳特伯生物医学成像研究中心，广东 深圳 518055；

[3]南方医科大学珠江医院肝胆一科，广东 广州 510282

摘要 声学分辨率光声显微技术具有较高的光学对比度和声学分辨率以及大穿透深度等优势，是一种具有广阔应用前景的生物医学成像技术。聚光镜聚焦与单侧侧面激发等传统的激发方式具有光斑不均匀、存在光学热噪点、光能利用率低等不足，在一定程度上限制了声学分辨率光声显微技术的临床前和临床应用。本团队通过改进声学分辨率光声显微镜的激发方式，由单侧激发改为双侧激发，提升了成像过程中光束对复杂生物组织的覆盖面积，从而提升了成像质量。结果表明，双侧激发方式使得声学分辨率光声显微镜在复杂生物样品成像过程中可以获得更高的对比度和信噪比，成像性能更好。

关键词 生物光学；光声显微成像；声学分辨率；双侧激发

中图分类号 Q631 **文献标志码** A **DOI**：10.3788/CJL202249.1507201

1 引 言

近年来，光声成像技术作为一种新兴的生物医学成像技术得到了快速发展，其具有光学成像高对比度及声学成像高分辨率、高穿透深度的特点，突破了传统光学成像在生物医学成像应用方面的局限，在临床疾病诊断领域具有广阔的应用前景[1-5]。光声显微成像是光声成像技术的重要实现方式之一。根据成像系统中光束焦斑与声束焦斑的相对大小，可将光声显微成像分为声学分辨率光声显微（AR-PAM）成像和光学分辨率光声显微（OR-PAM）成像[6-7]。与分辨率取决于光束焦斑大小的 OR-PAM 相比，AR-PAM 采用光学弱聚焦方式，激光照明样品区域较大，主要通过高频聚焦超声换能器获得较好的横向分辨率，且成像深度可达厘米级别，在复杂生物组织成像、深部肿瘤检测等生物医学应用中具有较大优势。

光声显微成像是一种无创的生物成像技术，能够获取跨尺度、多参量的生物医学信息，可在组织、器官、全身等多个水平实现跨尺度成像，可应用于肿瘤病理生理学、活体小动物血流动力学及药物动力学等研究[8-10]。利用不同生物组织对光的不同吸收特性可以无标记获取活体组织的高对比结构图像（如可以获得活体血管构象的改变[11]，还可以实现肿瘤边界界定[12]），同时结合光声光谱的差异，可以通过多波长测量定量分析活体组织的成分变化，实现功能成像（如可以对血氧浓度、氧代谢、血流速度[13]等生理参数进行测量）。近年来，各种特异性分子造影剂的开发使得光声显微成像的应用更为广泛[14-15]，但光在生物组织内的强散射使其应用受到限制。如何提升光声成像对生物深部组织的成像质量是当前的研究热点[16-17]。

尽管 AR-PAM 的成像分辨率主要取决于声焦斑的大小，但有效的光束照明对于获取高质量图像仍十分重要。目前，AR-PAM 系统的激发方式主要有两类：一类是由锥透镜产生环形光，通过聚光镜弱聚焦[18]；另一类是经由光纤传输，被透镜整形后直接照射于样品。前者由于光斑不均匀，光学热噪点较多，会影响图像质量，而且激光通过聚光镜后能量损失较大，成像灵敏度减弱。后者对激光的利用率高于前者，且采用光纤进行激发光耦合传输，大大增强了系统的灵活性；但该方法目前多采用单侧激发设计，在成像过程中，凹凸不平的生物组织表面使得光照不均匀，特别是对于具有非规则形状的复杂生物组织样本（比如肿瘤组织、脑、腿部等）的成像来说，受单侧激发的限制，激发光无法完整覆盖目标区域，难以呈现样品的全部形态，更难以获得深层组织的信息。

收稿日期：2021-12-24；**修回日期**：2022-02-08；**录用日期**：2022-02-28

基金项目：国家重点研发计划（2021YFE0202200，2020YFA0908800）、国家自然科学基金（82122034，92059108，81927807，81627805）

通信作者：*hr. zheng@siat. ac. cn；**cb. liu@siat. ac. cn

针对此问题，本团队提出了双侧激发的新方法。首先采用仿体实验验证该方法的可行性，然后采用该方法对小鼠腿部淋巴结、脑部血管及肿瘤新生血管进行成像，分析该方法的优势。实验结果表明，相对于单侧激发，双侧激发的AR-PAM系统对复杂生物样品的成像对比度更高，能够更加精准地呈现样品组织的完整边界，可以获取更全面的信息，在临床及临床前研究中具有潜在的应用价值。

2　方法与实验

2.1　双侧激发光声显微成像系统设计

图1(a)所示为双侧激发光声显微成像系统的示意图。采用重复频率为100 Hz、波长为780 nm的SpitLight EVO S OPO-100型纳秒脉冲激光器作为光声信号激发光源，激光器出射的光束经过衰减、扩束、准直后，由偏振分光器分为两束，两束光经由自制的光纤耦合器耦合进入纤芯直径为1500 μm的多模光纤，光纤出射的光束在成像探头处由平凸透镜整形后照射到成像样品区域[如图1(b)所示]。采用中心频率为25 MHz的V324-SU型高频超声换能器接收样品产生的光声信号。光声探头集成于由步进电机驱动的PSA2000-11型精密移动式三维扫描平台上，通过LabVIEW语言编写的上位机程序控制探头移动，进行栅格扫描。超声换能器将声信号转化为电信号后，由超声收发仪5073PR放大，接着被CS1422型双通道数据采集卡以100 MS/s的采样速率进行采集并存储到计算机中，然后在MATLAB环境下进行重建，即可得到光声图像。

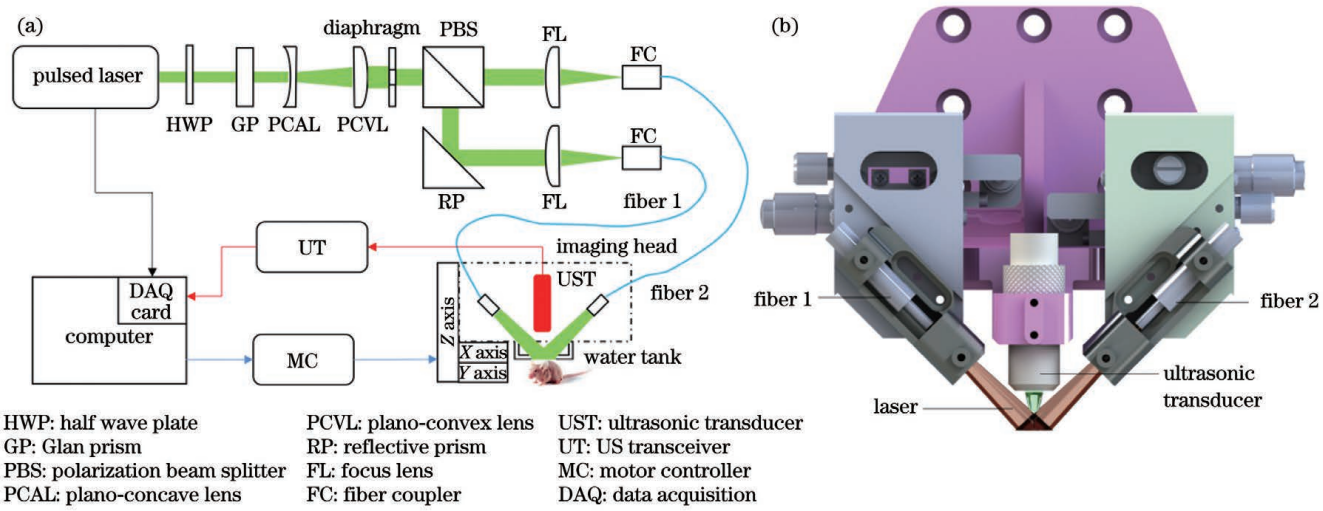

图1　双侧激发光声显微成像系统示意图。(a)成像系统方案设计图；(b)成像探头结构示意图

Fig. 1　Schematics of dual-sided illumination photoacoustic (PA) microscopy imaging system. (a) Schematic of imaging system; (b) structure schematic of imaging head

2.2　仿体实验设计

为了验证双侧激发方式相比于单侧激发的优势，本团队制作了两种仿体进行实验验证。

仿体1：将琼脂粉与去离子水按1∶100的质量比混匀加热，浇筑成半球形凝胶仿体；将直径为1 mm的锡丝制成圆锥螺旋线状，并将其固定于仿体表面，用于模拟生物体组织内不同深度的血管；再在仿体表面覆盖琼脂溶液，待其冷却成型即可。

仿体2：将琼脂粉与去离子水按1∶100的质量比混匀加热，浇筑成半球形凝胶仿体；冷却成型后，将5根不同弧度、直径为1 mm的锡丝平行固定于仿体表面；再将混有2%脂肪乳溶液的琼脂混合液均匀覆盖于仿体表面。该仿体用于模拟生物组织对光的散射作用。

首先进行双侧激发成像实验，即：在仿体表面涂抹超声耦合胶后，将其置于水槽下方，控制电机使超声换能器探头对焦于仿体最高点，并使探头左右两侧的激发光都照射到样品表面，调节激发光的强度，使样品表面的激光能量密度为5.5 mJ/cm^2，进行栅格扫描。然后进行单侧激发成像实验，即：将成像探头返回扫描原点，遮蔽一侧激发光，调节激发光的强度，使样品表面的激光能量密度为5.5 mJ/cm^2，不改变样品的位置，进行栅格扫描。在MATLAB环境下，对采集的数据进行最大值投影图像(MAP)重建及分析。

2.3　小鼠活体实验设计

为了进一步验证双侧激发方式在复杂生物样本成像上的优势，分别对小鼠腿部淋巴结、脑部血管及肿瘤实施了双侧激发与单侧激发方式的光声显微实验，并对实验结果进行进一步分析与比较。

使用4～6周龄、体重为18～20 g、品系为Balb/c的雄性裸鼠(北京维通利华实验动物技术有限公司)建立肿瘤模型并进行活体光声成像。裸鼠脑部血管的光声成像采用无标记、无创的成像方式。

腿部淋巴结的成像模拟临床注射吲哚菁绿(ICG)示踪前哨淋巴结的方法，即：通过裸鼠后肢足垫注射

50 μL质量浓度为1 mg/mL的ICG溶液，30 min后对后肢进行成像。

使用人源肝癌细胞系Hep G2建立小鼠皮下瘤模型，即：将Hep G2细胞置于添加了10%（体积分数）胎牛血清、1%（体积分数）青霉素的DMEM培养基中，并置于37 ℃、5%（体积分数）CO_2的环境下培养孵育，取对数期生长的细胞，由皮下注射至小鼠下肢背侧建模。

在成像过程中，采用Matrx VMR型小动物麻醉机将一定体积分数的异氟烷（3%，用于诱导；1%～2%用于维持）混入氧气（1 L/min）中对实验小鼠实施麻醉，并采用69020型体温控制器使小鼠的体温维持在37 ℃。活体成像时，照射在小鼠皮肤上的单脉冲激光能量约为3 mJ，光能量密度约为16 mJ/cm^2，低于美国国家标准协会（ANSI）规定的安全阈值20 mJ/cm^2。实验过程中的所有操作均按照中国科学院深圳先进技术研究院动物研究委员会批准的方案进行。

3 结果与讨论

3.1 仿体光声显微成像结果

单侧与双侧激发方式示意图如图2所示，其中图2(a)、(c)为单侧激发，图2(b)、(d)为双侧激发。在成像过程中，声信号焦平面位于样品表面。当探头位于样品最上方时，单侧激发与双侧激发光均能照射于样品表面并产生光声信号。当超声换能器探头沿x轴移动扫描时，若采用单侧激发，就会出现光的方向与样品表面相切及相离的情况，如图2(c)所示，导致超声换能器探头下方光束的会聚减弱或无光束会聚，因此该区域的光声信号减小，图像信噪比降低；而将激发方式改为双侧激发后，不论样品表面是否平整，在目标区域内探，头下方均有光束照明，均能激发出光声信号，如图2(d)所示，整体成像质量得以提升。

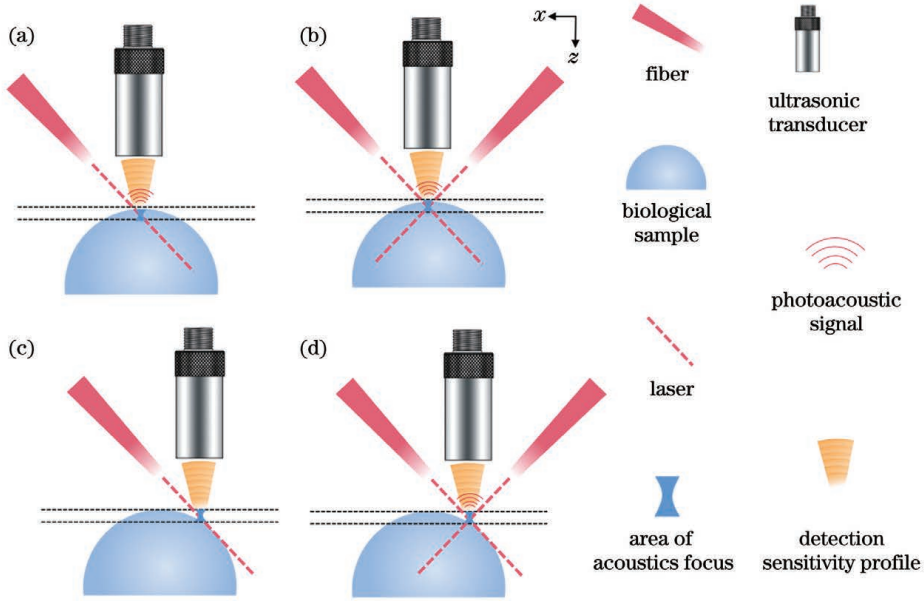

图2 不同激发方式在复杂生物样本不同部位成像的示意图。(a)(c)单侧激发；(b)(d)双侧激发

Fig. 2 Schematics of imaging different parts of complex biological samples by different illumination modes. (a)(c) Single-sided illumination; (b)(d) dual-sided illumination

在仿体1中，锡丝呈圆锥螺旋线状，如图3(a)所示。比较图3(b)、(c)可知，与单侧激发方案相比，在相同的激光能量密度下，双侧激发方案下MAP图像的整体信噪比更高。图3(d)所示曲线分别是图3(b)、(c)中虚线位置处信号的强度值。在成像过程，单侧激发在边缘区域对光束的会聚作用减弱，因此成像对比度下降。

为了进一步验证双侧激发的优势，本团队制作了仿体2，如图3(e)所示，用其模拟生物组织对光的散射作用。分析对比图3(f)～(h)可知：即使在强散射介质中，双侧激发方式依旧可以解析出复杂样品的完整轮廓，而单侧激发方式对仿体边缘锡丝的成像效果较差；双侧激发可以提升对深部血管仿体的成像能力[图3(h)所示曲线分别为图3(f)、(g)虚线位置处的信号强度值]，同时对于边缘较为靠近表层的血管仿体，也能获得更好的对比度[如图3(h)中的紫色、红色箭头所示]。仿体成像实验的结果验证了双侧激发方式进行显微成像的可行性。采用双侧激发方式进行显微成像不仅可以获取复杂样品的完整轮廓信息和深层信息，还可以进一步提高图像的对比度，实现更好的成像质量。

3.2 活体光声显微成像

为了进一步验证双侧激发方式在复杂生物样本成像中的优势，本团队进行了活体成像实验。

前哨淋巴结的精准示踪与定位是临床肿瘤诊治的重要需求之一[19-20]。术前通过影像学对前哨淋巴结进行示踪定位，不仅有利于手术的精准切除，还可以降低术中大面积清扫淋巴结所导致的创伤。目前，前哨

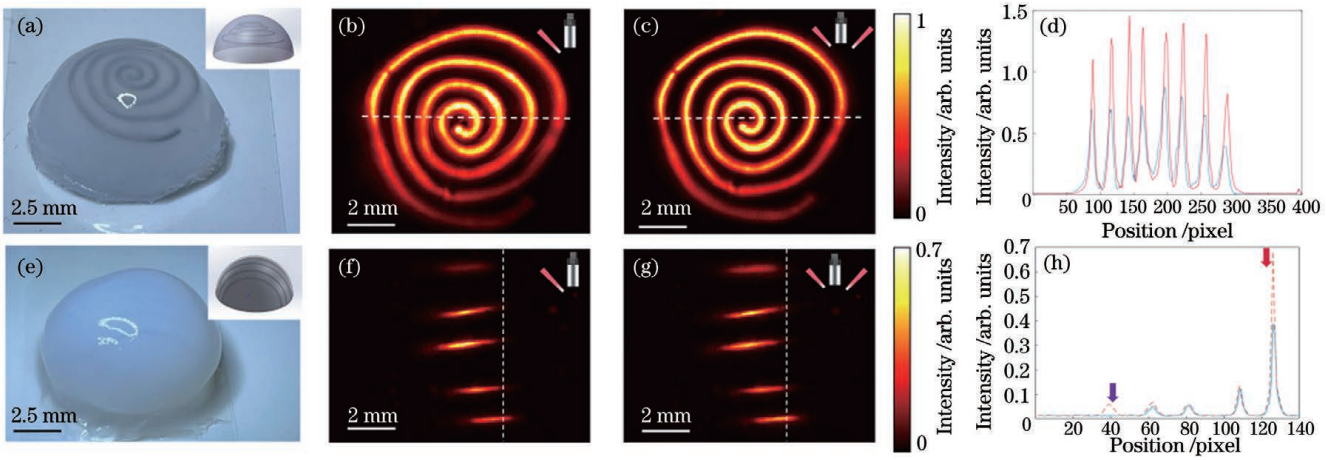

图3　不同激发方式下两种仿体的测试结果。(a)仿体1实物图;(b)仿体1在单侧激发方式下的光声MAP图;(c)仿体1在双侧激发方式下的光声MAP图;(d)仿体1在两种激发方式下的光声信号定量结果;(e)仿体2实物图;(f)仿体2在单侧激发方式下的光声MAP图;(g)仿体2在双侧激发方式下的光声MAP图;(h)仿体2在两种激发方式下的光声信号定量结果(红线:双侧激发;蓝线:单侧激发)

Fig. 3　Imaging results of two phantoms under different illumination modes. (a) Photo of phantom 1; (b) PA MAP of phantom 1 with single-sided illumination; (c) PA MAP of phantom 1 with dual-sided illumination; (d) quantitative results of photoacoustic signal of phantom 1 under two illumination modes; (e) photo of phantom 2; (f) PA MAP of phantom 2 with single-sided illumination; (g) PA MAP of phantom 2 with dual-sided illumination; (h) quantitative results of photoacoustic signal of phantom 2 under two illumination modes (red line: dual-sided illumination; blue line: single-sided illumination)

淋巴结的定位方法是:在目标区域注射ICG,通过局部淋巴管回流实现定位[21-23]。在本研究中,本团队通过足垫注射ICG的方法模拟临床上前哨淋巴结的染色定位,并比较两种激发方式的成像差异。

裸鼠的腘窝淋巴结位于后肢边缘腿部侧方皮下腘窝中[24],如图4(a)、(b)所示。采用单侧激发时,组织对光的强散射以及生物组织的遮挡等,导致淋巴结的显影特异性不高,如图4(c)~(d)所示。而对于双侧激发,当探头扫描小鼠后肢侧面区域时,光束依旧可以照射到边缘处,而且组织的散射对成像的影响较小,因此图像中淋巴结的光声信号更强,如图4(e)~(f)所示。对两种激发方式下的信号强度进行定量分析,结果显示,双侧激发方式下淋巴结的信号强度约为单侧激发方式下的3倍,如图4(g)所示。此外,本团队

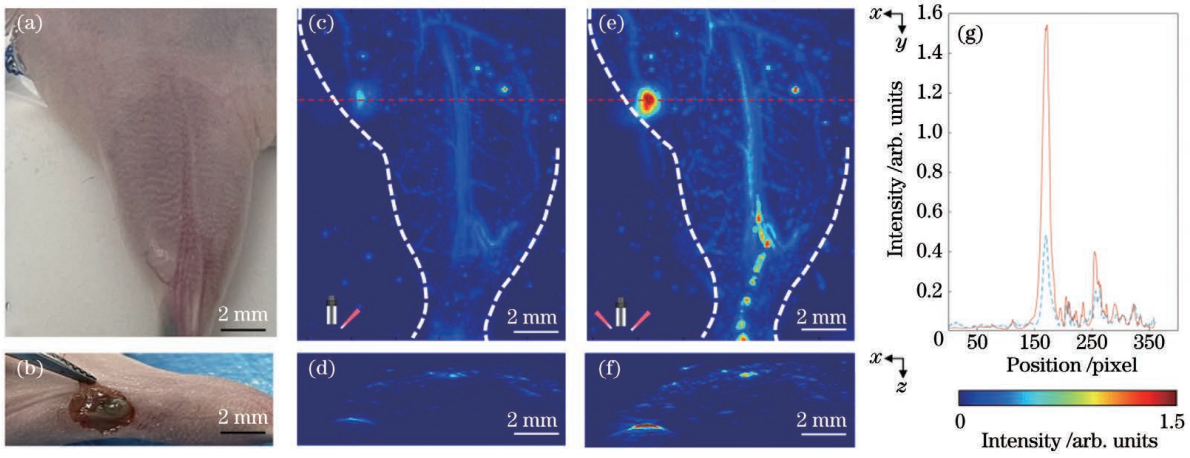

图4　健康小鼠腿部淋巴结在不同激发方式下的成像结果。(a)小鼠腿部实物图;(b)ICG染色淋巴结实物图;(c)单侧激发方式下小鼠腿部淋巴结的光声MAP图;(d)单侧激发方式下小鼠腿部淋巴结的光声B-scan图;(e)双侧激发方式下小鼠腿部淋巴结的光声MAP图;(f)双侧激发方式下小鼠腿部淋巴结的光声B-scan图;(g)图4(c)、(e)中红色虚线处光声信号强度的幅值(红线:双侧激发;蓝线:单侧激发)

Fig. 4　Imaging results of leg lymph nodes in healthy mouse under different illumination modes. (a) Photo of mouse leg; (b) photo of ICG stained lymph nodes; (c) PA MAP of mouse leg lymph nodes with single-sided illumination; (d) PA B-scan image of mouse leg lymph nodes with single-sided illumination; (e) PA MAP of mouse leg lymph nodes with dual-sided illumination; (f) PA B-scan image of mouse leg lymph nodes with dual-sided illumination; (g) amplitude of photoacoustic signal intensity along red dotted line in Figs. 4(c) and 4(e), where red line represents dual-sided illumination and blue line represents single-sided illumination

分析了两种成像方式的 B-scan 图，如图 4(d)、(f)所示。可以看出，对于侧面的成像，双侧激发可以呈现出更为明显的组织边缘以及更为丰富的血管信息。

3.3 小鼠脑皮层血管的光声成像

大脑皮层血管病变与多种疾病相关，脑皮层血管的高效无创成像对于临床诊疗意义重大。目前，可用于脑部血管成像的手段包括 CT 血管造影(CTA)、磁共振血管成像(MRA)等，但这些成像手段存在电离辐射或扫描速度慢、设备昂贵，以及无法对体内有金属植入物的患者进行扫描等不足[25]。光声脑皮层血管成像通过体内血红蛋白这一内源性造影剂可以实现特异性血管精准成像。由于脑实质呈半球状，以往的单侧激发存在弊端，在扫描过程中易导致目标区域边缘的光束照明不足，从而影响成像质量。图 5(a)、(d)分别为双侧激发与单侧激发光声显微成像的 MAP 图，图 5(b)、(e)为其放大图。可见，双侧激发可以呈现出脑皮质中丰富的微小血管，而且血管信号的对比度更高。通过比较图 5(c)、(f)所示的 B-scan 图可以发现左侧成像不受激发方式的影响，但单侧激发方式下小鼠脑部右侧的光声信号缺失，如虚线框所示。图 5(g)所示为放大图中虚线所在位置的光声信号的幅值图。如红色箭头所示，同样的微血管在双侧激发下的对比度增大；如紫色箭头所示，单侧激发在边缘区域因照明不足而导致部分微血管未被检测到。

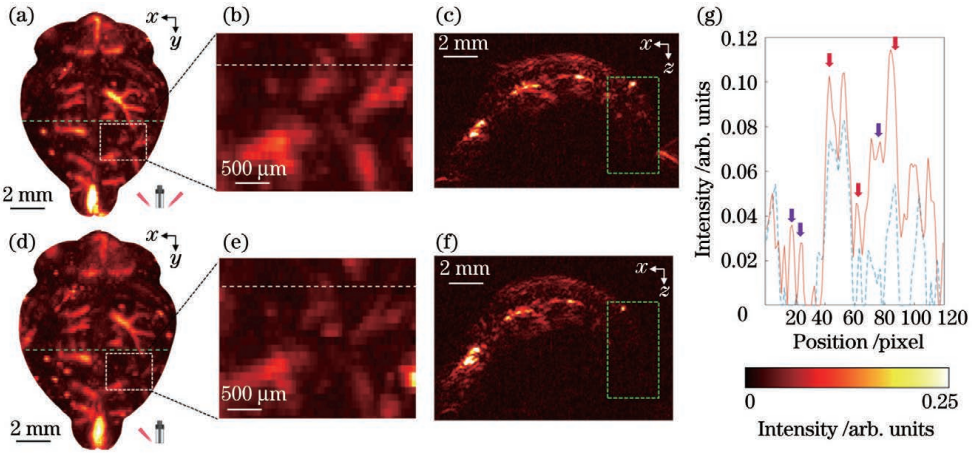

图 5　健康小鼠脑部血管在不同激发方式下的无标记成像结果。(a)双侧激发方式下健康小鼠脑部血管的光声 MAP 图；(b)图 5(a)方框区域的放大图；(c)图 5(a)虚线处的光声 B-scan 图；(d)单侧激发方式下健康小鼠脑部血管的光声 MAP 图；(e)图 5(d)方框区域的放大图；(f)图 5(d)虚线处的光声 B-scan 图；(g)不同激发方式下光声信号的幅值(红线：双侧激发；蓝线：单侧激发)

Fig. 5 Label free imaging results of brain vessels of a healthy mouse with different illustration modes. (a) PA MAP image of brain vessels of a healthy mouse with dual-sided illumination; (b) enlarged box area in Fig. 5 (a); (c) PA B-scan image of dotted line in Fig. 5 (a); (d) PA MAP image of brain vessels of a healthy mouse with single-sided illumination; (e) enlarged box area in Fig. 5 (d); (f) PA B-scan image of dotted line in Fig. 5 (d); (g) amplitude of photoacoustic signal intensity with different illumination modes, where red line represents dual-sided illumination and blue line represents single-sided illumination

3.4 小鼠肿瘤光声成像

肿瘤是目前严重威胁人类健康的公共卫生问题之一。由于缺乏对肿瘤演变过程病理及生化代谢的精准检测及干预，目前肿瘤患者的整体预后仍不理想，因此，准确完整地对实体肿瘤进行成像具有重要意义。近年来，基于小动物的肿瘤光声成像是研究的热点方向[26-27]。AR-PAM 以其较大的穿透深度和较高的图像分辨率在肿瘤组织的结构及功能成像上具有显著优势。实体肿瘤表面多呈凸起状，这会使成像过程照明不均匀，从而导致成像结果不准确。此外，对肿瘤上新生供血血管的评估是临床治疗方案制订的重要参考依据[28-30]，若新生滋养血管成像不准确，就会影响治疗方案的制订。

本团队通过对荷瘤小鼠进行无标记活体成像来验证双侧激发方式对肿瘤成像的可行性。为了评估肿瘤周围滋养血管的差异，将超声换能器的焦斑调整至肿瘤基底，进行信号采集。图 6(a)、(b)为同一只荷瘤小鼠相同部位、相同深度处肿瘤在两种激发方式下的光声 MAP 图像，其中白色虚线圆圈表示肿瘤位置。可见，在单侧激发下，肿瘤右侧仅可见稀疏的粗血管，而在双侧激发下，同一区域的血管显示得更加丰富，可以看到更多的细小滋养血管。

为了进一步验证双侧激发对实体肿瘤边界成像的优势，本团队采集了另一只荷瘤小鼠体内肿瘤的光声图像，并进行三维重建分析。在采集过程中，将超声换能器探头的焦斑移至实体肿瘤处，以更好地获得肿瘤的轮廓信号。由图 6(c)、(e)可以看出：肿瘤的滋养血管位于右侧(如绿色箭头所示)，双侧激发下可见对比度更高的血管图像；对于右侧的肿瘤，其轮廓在双侧激发方案下显示得更加完整(如黄色箭头所示)。在图 6(d)、(f)所示的三维重建图像中也可以看出双侧激发能够更为完整地采集肿瘤的光声图像。

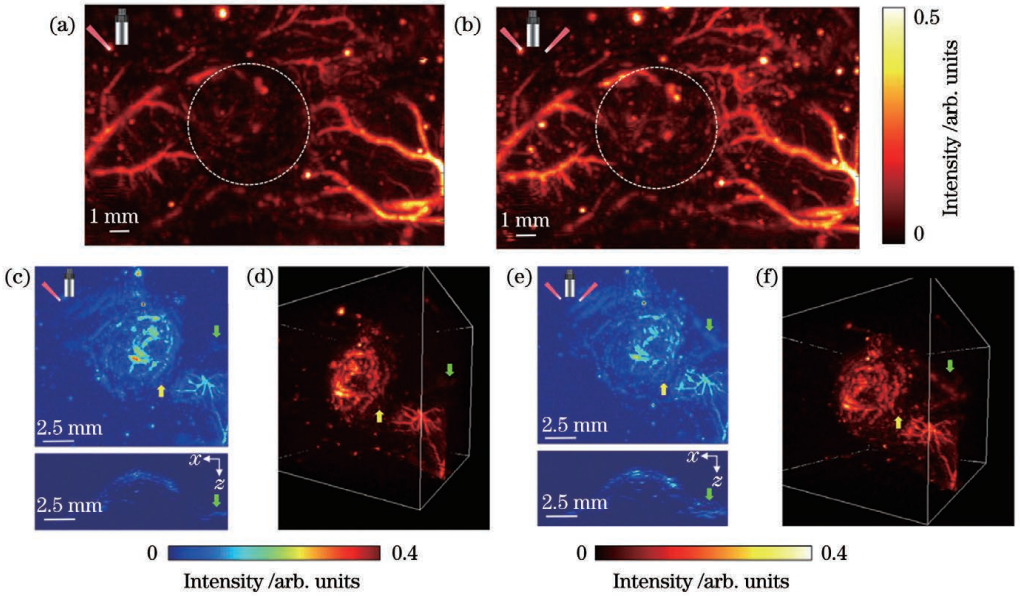

图 6　荷瘤小鼠肿瘤区在不同激发方式下的无标记成像结果(绿色箭头:肿瘤滋养血管;黄色箭头:肿瘤边缘)。(a)单侧激发方式下小鼠肿瘤基底血管的光声 MAP 图(虚线圆圈为肿瘤区域);(b)双侧激发方式下小鼠肿瘤基底血管的光声 MAP 图;(c)单侧激发方式下小鼠肿瘤区的光声 MAP 图及 B-scan 图;(d)图 6(c)的三维重建结果;(e)双侧激发方式下小鼠肿瘤区的光声 MAP 图及 B-scan 图;(f)图 6(e)的三维重建结果

Fig. 6　Label free imaging results of mouse tumor area with different illustration modes (green arrow: tumor nourishing blood vessel; yellow arrow: tumor edge). (a) PA MAP image of mouse basal tumor vessels with single-sided illumination (the dotted circle is tumor area); (b) PA MAP image of mouse basal tumor vessels with dual-sided illumination; (c) PA MAP and B-scan images of mouse tumor area with single-sided illumination; (d) three-dimensional reconstruction result of Fig. 6(c); (e) PA MAP and B-scan images of mouse tumor area with dual-sided illumination; (f) three-dimensional reconstruction result of Fig. 6(e)

综上可得:在 AR-PAM 成像中,使用双侧激发的方式更具有优势,能够得到对比度更高的肿瘤边缘滋养血管图像;双侧激发方式由于减少了组织对入射光的散射,得到的肿瘤的轮廓也更为完整,能够更好地应用于临床及临床前对肿瘤的研究。

4　结　　论

本团队提出了一种适用于复杂生物样品精准光声显微成像的方法,利用双侧激发的方式,实现了复杂生物样品的精准显微成像。通过仿体成像实验验证了双侧激发的可行性,并将其应用于活体裸鼠下肢淋巴结的精准定位以及脑实质血管的无创无标记成像。与传统的激发方式(单侧激发)相比,在对肿瘤滋养血管的成像中,双侧激发能够对肿瘤边缘的微小血管实现高对比度成像,实现了荷瘤小鼠肿瘤边界的准确界定。双侧激发方式相比传统锥透镜式及单侧激发式 AR-PAM,能够更为精准地实现复杂生物样品的光声成像,为光声显微成像技术应用于临床和临床前的精准诊断提供了新方法。

参　考　文　献

[1]　张芬, 张吴昱, 李春澍, 等. 光声显微成像引导注射微整形术研究[J]. 中国激光, 2021, 48(21): 2107002.
Zhang F, Zhang W Y, Li C S, et al. Photoacoustic microscopy for injection navigation of microplastic surgery [J]. Chinese Journal of Lasers, 2021, 48(21): 2107002.

[2]　Wang L V, Yao J. A practical guide to photoacoustic tomography in the life sciences[J]. Nature Methods, 2016, 13(8): 627-638.

[3]　Wong T T W, Zhang R Y, Hai P F, et al. Fast label-free multilayered histology-like imaging of human breast cancer by photoacoustic microscopy [J]. Science Advances, 2017, 3(5): e1602168.

[4]　龙晓云, 田超. 生物医学光声显微成像: 技术和应用进展[J]. 中国激光, 2020, 47(2): 0207016.
Long X Y, Tian C. Biomedical photoacoustic microscopy: advances in technology and applications[J]. Chinese Journal of Lasers, 2020, 47(2): 0207016.

[5]　李娇, 李帅, 陈冀景, 等. 非接触光声成像研究进展及其在生物医学上的应用[J]. 中国激光, 2021, 48(19): 1918005.
Li J, Li S, Chen J J, et al. Progress and biomedical application of non-contact photoacoustic imaging [J]. Chinese Journal of Lasers, 2021, 48(19): 1918005.

[6]　陈宁波, 周慧超, 赵煌旋, 等. 肿瘤血管的高分辨光声定量成像[J]. 中国激光, 2019, 46(9): 0907001.
Chen N B, Zhou H C, Zhao H X, et al. High-resolution photoacoustic quantitative imaging of tumor vessels[J]. Chinese Journal of Lasers, 2019, 46(9): 0907001.

[7]　Park S, Lee C, Kim J, et al. Acoustic resolution photoacoustic microscopy[J]. Biomedical Engineering Letters, 2014, 4(3): 213-222.

[8]　Mai T T, Yoo S W, Park S, et al. *In vivo* quantitative vasculature segmentation and assessment for photodynamic therapy process monitoring using photoacoustic microscopy[J]. Sensors, 2021, 21(5): 1776.

[9]　Baik J W, Kim J Y, Cho S, et al. Super wide-field photoacoustic microscopy of animals and humans *in vivo* [J]. IEEE Transactions on Medical Imaging, 2020, 39(4): 975-984.

[10] Johnson S P, Ogunlade O, Lythgoe M F, et al. Longitudinal photoacoustic imaging of the pharmacodynamic effect of vascular targeted therapy on tumors[J]. Clinical Cancer Research: an Official Journal of the American Association for Cancer Research, 2019, 25(24): 7436-7447.
[11] Wang Z, Yang F, Ma H, et al. Bifocal 532/1064 nm alternately illuminated photoacoustic microscopy for capturing deep vascular morphology in human skin[J]. Journal of the European Academy of Dermatology and Venereology, 2022, 36(1): 51-59.
[12] Wang C C, Guo L L, Wang G, et al. *In-vivo* imaging of melanoma with simultaneous dual-wavelength acoustic-resolution-based photoacoustic/ultrasound microscopy[J]. Applied Optics, 2021, 60(13): 3772-3778.
[13] Chen S L, Xie Z X, Carson P L, et al. *In vivo* flow speed measurement of capillaries by photoacoustic correlation spectroscopy[J]. Optics Letters, 2011, 36(20): 4017-4019.
[14] Chen J Q, Qi J, Chen C, et al. Tocilizumab-conjugated polymer nanoparticles for NIR-II photoacoustic-imaging-guided therapy of rheumatoid arthritis[J]. Advanced Materials, 2020, 32(37): 2003399.
[15] 巩飞, 程亮, 刘庄. 基于纳米探针的肿瘤光声成像研究[J]. 激光与光电子学进展, 2020, 57(18): 180004.
Gong F, Cheng L, Liu Z. Application of nanoprobes in photoacoustic cancer imaging[J]. Laser & Optoelectronics Progress, 2020, 57(18): 180004.
[16] Lai P X, Wang L D, Tay J W, et al. Photoacoustically guided wavefront shaping for enhanced optical focusing in scattering media[J]. Nature Photonics, 2015, 9(2): 126-132.
[17] Cheng S F, Zhou Y Y, Chen J B, et al. High-resolution photoacoustic microscopy with deep penetration through learning[J]. Photoacoustics, 2022, 25: 100314.
[18] Zhang H F, Maslov K, Stoica G, et al. Functional photoacoustic microscopy for high-resolution and noninvasive *in vivo* imaging[J]. Nature Biotechnology, 2006, 24(7): 848-851.
[19] Matsuda S, Irino T, Kawakubo H, et al. Current status and challenges in sentinel node navigation surgery for early gastric cancer[J]. Chinese Journal of Cancer Research, 2021, 33(2): 150-158.
[20] Lee C M, Park S, Park S H, et al. Sentinel node mapping using a fluorescent dye and visible light during laparoscopic gastrectomy for early gastric cancer[J]. Annals of Surgery, 2017, 265(4): 766-773.
[21] Jimenez-Lillo J, Villegas-Tovar E, Momblan-Garcia D, et al. Performance of indocyanine-green imaging for sentinel lymph node mapping and lymph node metastasis in esophageal cancer: systematic review and meta-analysis[J]. Annals of Surgical Oncology, 2021, 28(9): 4869-4877.
[22] Zhong Q, Chen Q Y, Huang X B, et al. Clinical implications of indocyanine green fluorescence imaging-guided laparoscopic lymphadenectomy for patients with gastric cancer: a cohort study from two randomized, controlled trials using individual patient data[J]. International Journal of Surgery, 2021, 94: 106120.
[23] Kedrzycki M S, Leiloglou M, Ashrafian H, et al. Meta-analysis comparing fluorescence imaging with radioisotope and blue dye-guided sentinel node identification for breast cancer surgery[J]. Annals of Surgical Oncology, 2021, 28(7): 3738-3748.
[24] van den Broeck W, Derore A, Simoens P. Anatomy and nomenclature of murine lymph nodes: descriptive study and nomenclatory standardization in BALB/cAnNCrl mice[J]. Journal of Immunological Methods, 2006, 312(1/2): 12-19.
[25] Kidwell C S, Hsia A W. Imaging of the brain and cerebral vasculature in patients with suspected stroke: advantages and disadvantages of CT and MRI[J]. Current Neurology and Neuroscience Reports, 2006, 6(1): 9-16.
[26] Liu Y J, Bhattarai P, Dai Z F, et al. Photothermal therapy and photoacoustic imaging via nanotheranostics in fighting cancer[J]. Chemical Society Reviews, 2019, 48(7): 2053-2108.
[27] Fu Q R, Zhu R, Song J B, et al. Photoacoustic imaging: contrast agents and their biomedical applications[J]. Advanced Materials, 2019, 31(6): 1805875.
[28] Zhang Q, Wu J J, Bai X L, et al. Evaluation of intra-tumoral vascularization in hepatocellular carcinomas[J]. Frontiers in Medicine, 2020, 7: 584250.
[29] Fu Z H, Zhang J, Lu Y J, et al. Clinical applications of superb microvascular imaging in the superficial tissues and organs: a systematic review[J]. Academic Radiology, 2021, 28(5): 694-703.
[30] Haedicke K, Agemy L, Omar M, et al. High-resolution optoacoustic imaging of tissue responses to vascular-targeted therapies[J]. Nature Biomedical Engineering, 2020, 4(3): 286-297.

Acoustic-Resolution Photoacoustic Microscopy with Dual-Sided Illumination

Zeng Silue[1,3], Liu Liangjian[1], Chen Tao[1], Fang Chihua[3], Liu Chengbo[1**], Zheng Hairong[2*]

[1] *Research Lab for Biomedical Optics and Molecular Imaging, Shenzhen Institute of Advanced Technology, Chinese Academy of Sciences, Shenzhen* 518055, *Guangdong, China*;

[2] *Paul C. Lauterbur Research Center for Biomedical Imaging, Shenzhen Institute of Advanced Technology, Chinese Academy of Sciences, Shenzhen* 518055, *Guangdong, China*;

[3] *First Department of Hepatobiliary Surgery, Zhujiang Hospital, Southern Medical University, Guangzhou* 510282, *Guangdong, China*

Abstract

Objective Photoacoustic imaging (PAI) is an emerging biomedical imaging technique with a high contrast of optical imaging and high resolution and deep penetration of acoustic imaging, which has shown broad application prospects in the field of clinical disease diagnosis. An important implementation for realizing PAI is using acoustic-resolution photoacoustic microscopy (AR-PAM). Conventional light illumination methods have the problem of uneven light distribution, optical thermal noise, large energy loss, and decreased imaging sensitivity. Additionally, for the samples of complex biological tissues with irregular shapes, such as tumor and brain tissues, single-sided illumination methods have imaging limitations

such as incomplete coverage of the target area and difficulty in obtaining accurate deep tissue information. In this paper, we report a dual-sided illumination method for AR-PAM. When compared with conventional methods, this method has higher imaging contrast in complex biological samples and can more accurately present the complete boundary of sample tissue. More comprehensive information was obtained, demonstrating the method's promising potential in both clinical and preclinical research.

Methods A polarization splitter was used in this study to divide the laser beam into two beams and they were coupled into the multimode optical fiber through fiber couplers. After being shaped with a planoconvex lens on both sides of an imaging probe, the emitted beams were irradiated to the imaging sample at a 45° angle. A high-frequency ultrasonic transducer received the photoacoustic signals generated by the sample. First, the feasibility of imaging was verified by creating two phantoms mimicking blood vessels at different depths. The imaging of popliteal lymph nodes, brain vasculature, and tumors in living mice with two illumination methods was then performed and compared, and their imaging performance with dual-sided illumination was more excellent than that with single-sided illumination method, proving the advantages of dual-sided illumination method in PAI of complex biological samples.

Results and Discussions When the PAI results of the two tissue phantoms under different illumination schemes are compared, the overall signal-to-noise ratio and contrast of the images in the dual-sided illumination method are found to be better than those in the single-sided illumination method and more complete contour and depth information can be obtained for the imaging of complex samples (Fig. 3). In *in vivo* imaging experiments, the advantages of dual-sided illumination in improving imaging quality are also verified. Through imaging of indocyanine green traced (ICG-traced) mouse popliteal lymph nodes, the signal intensity of lymph nodes using dual-sided illumination method was approximately three times higher than that using the single-sided illumination method (Fig. 4). Noninvasive imaging of cerebral cortical blood vessels showed that the dual-sided illumination method can present more abundant microvessels in the marginal region with higher contrast (Fig. 5). Unlabeled *in vivo* imaging of mouse tumors was performed to evaluate the differences in peripheral vascular imaging between the two illumination methods, and the results showed that the blood vessels observed in the same area using the dual-sided illumination method were more abundant and tumor nourishing vessels were visible (Fig. 6). In addition, three-dimensional reconstruction of the tumor image showed that the dual-sided illumination method can image tumor edges more accurately and completely.

Conclusions In this study, the imaging quality is improved by reconfiguring the light illumination method of AR-PAM from single-sided illumination to dual-sided illumination to achieve the homogeneous coverage of a laser beam for imaging complex biological tissues. The results show that the dual-sided illumination method improves contrast and signal-to-noise ratio for PAI in complex biological samples such as tissue phantoms, popliteal lymph nodes, brain vasculature, and tumors. Our study provides a new method for photoacoustic microscopy and has the potential to improve diagnosis accuracy in clinical and preclinical practices.

Key words bio-optics; photoacoustic microscopy; acoustic resolution; dual-sided illumination